PNAS RESEARCH ARTICLE | CLASSIFICATION

Climate mitigation contributes more to population persistence than evolutionary adaptation in a long-lived seabird

Stéphanie Jenouvrier[a,2], Jimmy Garnier[b], Marika Holland[c], Joanie van de Walle[d], Samantha C. Patrick[e], Timothée Bonnet[f], Karine Delord[f], Francesco Ventura[a], Christophe Barbraud[f], and Henri Weimerskirch[f]

This manuscript was compiled on June 8, 2026

Evolutionary rescue—the process by which adaptive evolution prevents population extinction following environmental deterioration (1, 2)—is frequently proposed as a buffer against biodiversity loss under climate change, yet its capacity to alter future population trajectories is rarely assessed quantitatively (3–5). Most forecasts of evolutionary rescue rely on simplified demographic models (6), focus on a single adaptive trait (4, 5), and explore hypothetical environmental scenarios rather than standardized climate pathways (7), neglecting uncertainty from demographic and internal climate variability (8). We developed a hyperstate eco-evolutionary population model (9) coupled with large ensembles of climate projections from global climate models (10) to test whether evolutionary adaptation or climate mitigation can prevent declines in a threatened seabird, the black-browed albatross. We parameterized this framework using three decades of demographic and phenotypic data (11), while propagating uncertainty from demographic processes and natural climate variability in climate projections (10). We evaluated selection on morphological, behavioural, and phenological traits influencing different life-cycle components across contrasting climate scenarios. Evolution increased population size under stationary historical climates but failed to prevent decline under projected warming. Increasing heritability had little effect on extinction risk, whereas climate mitigation reduced extinction probability by approximately half. Evolutionary rescue occurred only under the most optimistic climate scenario when climate change directly strengthened selection on wing length, a trait affecting juvenile survival. Our results reveal limits to evolutionary rescue under environmental change.

Evolutionary rescue | Eco-evolutionary forecasting | Climate change | Population persistence | Climate mitigation

Significance

Can species evolve fast enough to avoid extinction under climate change? We developed an eco-evolutionary forecasting framework that integrates quantitative genetics, demographic processes, and climate projections to address this question in a long-lived seabird. By examining morphological, behavioral, and phenological traits affecting different life-cycle stages, we show that adaptive evolution increased population growth under historical climates but failed to prevent decline under projected warming. Climate mitigation reduced extinction risk far more than evolutionary adaptation, while evolutionary rescue (the prevention of extinction through adaptation) occurred only when climate change strengthened selection on a trait affecting juvenile survival. These results reveal important limits to evolutionary rescue under rapid environmental change.

Predicting how species will respond to rapid climate change is one of the most pressing challenges in ecology and evolutionary biology (12–14). Although evolutionary adaptation can sometimes offset environmental deterioration and promote population persistence, whether it can keep pace with contemporary climate change remains highly uncertain (3, 15, 16). This question is particularly acute for long-lived species, where generation times are long and evolutionary responses may unfold more slowly than demographic declines (7).

Addressing this challenge requires forecasting frameworks that integrate climate projections developed for Intergovernmental Panel on Climate Change (IPCC) assessments with demographic and evolutionary processes (6). However, most forecasts of evolutionary rescue rely on simplified assumptions. They typically focus on a single adaptive trait (4, 5), use statistical approaches such as the breeder's equation to predict evolutionary change without explicitly embedding demographic processes (6), and often explore hypothetical environmental scenarios rather than standardized climate pathways (7). In addition, previous studies neglect uncertainty arising from demographic processes and internal climate variability.

Author affiliations: [a]Biology, Woods Hole Oceanographic Institution, Woods Hole, MA 02543, USA; [b]LAMA, CNRS–Université Grenoble Alpes, Université de Savoie Mont Blanc, Chambéry 73370, France; [c]Climate and Global Dynamics Laboratory, National Center for Atmospheric Research, Boulder, CO 80305, USA; [d]Biology, University of Rimouski, Rimouski, QC G5L 3A1, Canada; [e]School of Environmental Sciences, University of Liverpool, Liverpool L69 3GP, United Kingdom; [f]Centre d'Études Biologiques de Chizé, UMR7372, CNRS–La Rochelle Université, Villiers-en-Bois 79360, France

S.J. conceived the research, designed the analyses, constructed the models, and performed the analyses. J.G. assisted in model construction. M.H. computed climate projections. J.V.d.W. and T.B. contributed to analysis design and data analysis. S.C.P. and F.V. assisted with model parameterization. K.D., C.B., and H.W. collected data. S.J. wrote the manuscript with input from all authors.

The authors declare no competing interests.

[2]To whom correspondence should be addressed. E-mail: sjenouvrier@whoi.edu

However, organisms possess multiple traits that differ in heritability and demographic influence (17–19), and climate trajectories themselves reflect substantial internal climate variability superimposed on anthropogenic forcing (10). Most studies of evolutionary rescue focus on a single phenotypic trait, chosen because it is expected to be most sensitive to climate change or to offer the greatest adaptive potential (4, 5). For example, in corals, selection acts primarily on thermal tolerance (5), while in great tits, evolution of breeding phenology temporarily reduced trophic mismatch but failed to prevent population collapse under future warming (4). However, even within a single species, climate-driven selection can act on multiple traits that differ in heritability and their relative contribution to population demography. Moreover, most forecasting studies link trait variation to a single component of fitness, whereas population persistence depends on how trait-mediated changes propagate across the entire life cycle (6, 17–19). Changes in one trait may enhance a given fitness component but be offset by opposing effects of other traits or by demographic compensation across life-history stages, resulting in little net effect on population growth (20).

Uncertainty in future climate trajectories is a fundamental constraint on forecasting population persistence (8, 21, 22). Projections for climate-sensitive species can range from moderate declines to near-complete collapse depending on the emission pathway considered, as illustrated by recent forecasts for emperor penguins (8) and coral reefs (5). However, beyond differences among emission pathways, populations experience substantial variability arising from the climate system itself (8). Internal climate variability can strongly modulate the timing, magnitude, and persistence of climate change experienced by individuals, altering both traits, demographic rates and the strength of selection. Robust forecasts therefore cannot rely on phenomenological scenarios (7). Instead, they must compare population responses across standardized climate pathways developed for IPCC assessments, which capture a plausible spectrum of future non-stationary conditions, while accounting for natural climate variability (22). Despite this necessity, very few eco-evolutionary forecasting studies have embedded population projections within climate projections developed for IPCC assessments (4, 5), and none have explicitly accounted for uncertainty arising from natural climate variability using large ensembles of climate projections (10).

Here we developed a hyperstate eco-evolutionary model (9) coupled to large-ensemble IPCC climate projections (10). We applied this framework to a long-lived vertebrate, the black-browed albatross (*Thalassarche melanophris*), for which long-term individual-based data link functional traits to demographic rates across the full life cycle (11). This approach allows us to evaluate whether adaptive evolution across multiple traits can buffer climate-driven population declines under future warming. The framework integrates quantitative genetics with state-structured demography (9), explicitly representing both additive genetic and environmental sources of phenotypic variation. Crucially, the model propagates uncertainty from both climate forcing and climate natural variability and demographic processes.

Previous work (11) showed that different traits influence distinct components of the life cycle. Wing length, a morphological trait shaped by developmental and environmental conditions, is positively associated with juvenile survival and recruitment, whereas variation in foraging behavior and breeding phenology primarily affects reproductive success. These demographic pathways differ markedly in their contribution to population growth. In black-browed albatrosses, projected population decline is driven largely by climate-induced reductions in juvenile survival under warming sea surface temperatures (11). Consequently, selection acting on wing length has the potential to influence the demographic process most strongly linked to future population persistence, whereas selection acting on behavioral and phenological traits is expected to operate primarily through reproductive performance. Building on this foundation, we explicitly consider four functional traits spanning morphological, behavioral, and phenological dimensions to evaluate how adaptation acting through different demographic pathways alters eco-evolutionary dynamics. These traits are also expected to differ in their heritability (the genetic contribution to phenotypic variance) and evolvability (the capacity to respond to selection) (23, 24).

Results

An Eco-Evolutionary Model Linking Climate, Heritable Genetic Variations, Traits, and Demography. To evaluate whether adaptive evolution can buffer climate-driven population declines, we developed a hyperstate eco-evolutionary matrix population model that explicitly tracks individuals jointly by breeding value, expressed phenotype and demographic state, (Fig. 1, (9), see Methods). The breeding value represents the additive genetic component of a trait that is transmitted across generations, while the phenotype reflects the combined effects of genetic inheritance and environmental influences.

The framework explicitly links morphological, behavioral, and phenological traits to survival and reproduction across the entire life cycle, capturing how climate-driven environmental change acts on populations through trait-dependent vital rates. To do so, the hyperstate structure classifies individuals simultaneously by their breeding value, phenotype, and demographic state, such that population dynamics emerge from transitions acting within and across these states (Fig. 1, Methods). Population projection is constructed from modular biological subprocesses describing survival and stage transitions, phenotypic change, reproduction and inheritance of breeding values (Supporting Information).

Adaptation Enables Population Growth Under a Historical Climate. We first parameterized the hyperstate eco-evolutionary model using empirical trait distributions, documented relationships between traits and vital rates, and state-structured demography (11), and examined a first climate-driven scenario in which climate conditions remain equal to historical conditions (Supporting Information). Specifically, we assumed that future SSTs would remain equal to the historical mean observed over 1986–2022, allowing us to isolate the demographic consequences of genetic adaptation in the absence of ongoing climate change. Because quantitative genetic parameters are difficult to estimate robustly in wild populations, we explored a broad range of heritability values spanning the plausible parameter space.

Under this historical-climate scenario, our results show that selection-driven evolutionary change in all traits can enable substantial population growth (Fig. 2A), even at modest adaptation rates (Fig. 2B). Activity and wing length exhibit the greatest potential for adaptive response and yield the largest demographic effects, consistent with their strong influence on population growth identified in previous analyses (11). Across intermediate heritability values for morphological and phenological traits in birds (e.g. $h^2 = 0.3$ (24)), selection on activity and wing length is projected to increase total population size by 22% and 38%, respectively, by 2100 under stationary climate conditions defined by the historical mean.

Climate Mitigation Delays Population Decline More Than Evolutionary Change. We next projected population trajectories under climate change by forcing the hyperstate eco-evolutionary model with large ensembles of climate projections (Fig. 1, (25)) representing a high-emission pathway (SSP3–7.0), and with a low-emission climate projections consistent with the Paris Agreement (2°C target, (26)). To span a wide range of potential evolutionary responses, we contrasted low and high heritability values ($h^2 = 0.1$ and 0.9), acknowledging that the upper bound represents an extreme, largely theoretical case (5, 27). The model reproduced the observed population trajectory from 2006 to the present, with observed population estimates falling within the envelope of climate-driven projections, supporting its use for forward projections under future climates (Figs. 3A–D, S1).

Across all traits and heritability values, evolutionary change alone was insufficient to prevent population decline under projected warming. Projected declines and extinction timing were largely insensitive to heritability, indicating that increasing the rate of evolutionary change did not alter population outcomes under climate change (Fig. 3). In contrast, climate mitigation consistently increased mean population size and delayed the timing of population extinction across all traits and heritability values.

Climate mitigation delayed the median year of quasi-extinction by approximately 8–12 years relative to evolutionary change alone (Fig. 3E). Despite modest demographic benefits from evolutionary change, the probability of quasi-extinction ($\geq$99% decline) by 2100 remained high under the high-emission scenario, ranging from 78–92% across traits and heritability values (Fig. 3F). Increasing heritability from 0.1 to 0.9 reduced extinction probability by only 5–10%. By contrast, climate mitigation reduced extinction probability by half, to 47–67% across traits even under low heritability. These patterns were consistent across all traits, demonstrating that climate mitigation promotes population persistence more effectively than evolutionary change under projected warming.

Evolutionary Rescue Requires Climate-Dependent Selection. The potential for evolutionary rescue is constrained by several factors in our model. In our baseline empirical based scenario, climate change does not directly modify trait–fitness relationships; instead, traits evolve only indirectly through their effects on demographic rates. In long-lived species such as black-browed albatrosses (generation time of 24 years (28)), this indirect pathway limits the pace at which evolutionary change can influence population trajectories (9).

To explore conditions under which population decline could be buffered by evolutionary rescue, we implemented alternative scenarios in which selective pressures on juvenile survival are directly linked to climate change (Supporting Information). Specifically, the strength of selection on wing length increases with climate warming (Fig. S2), representing a situation in which climate change directly alters the fitness advantage associated with morphological variation. This assumption is biologically plausible in a warming Southern Ocean, where strengthening and poleward-shifting westerly winds are expected to favor individuals with larger wings through improved soaring efficiency and reduced flight costs (29, 30).

Under this climate-dependent selection scenario, evolutionary rescue emerged only under a low-emissions climate trajectory and sufficiently strong evolutionary responses (Figs. 4, S3). With high heritability, the population increased from 2,390 individuals in 2006 to 3,657 individuals by 2100 (Fig. 4A), driven by a marked increase in juvenile survival (Fig. 4B). This demographic response was accompanied by a shift in the mean breeding value for wing length (Fig. 4C), which represents the average genetic contribution to the trait expressed in standardized units. This indicates a population shift toward genotypes associated with larger wings (Fig. 4D) and higher juvenile survival (Fig. 4B) under warmer conditions.

Evolutionary rescue occurred only when heritability exceeded a threshold value (approximately $h^2 \geq 0.3$; Fig. S4), below which populations continued to decline. This result defines a necessary threshold in heritable response for evolutionary rescue, and this threshold lies within the range of heritability estimates for morphological traits in birds (see Discussion (24)). Under high-emissions scenarios, evolutionary rescue did not occur regardless of heritability, with population declines beginning in the 2030s in all cases (Fig. S3). This outcome reflects the combined negative effects of warming on adult breeding success and juvenile recruitment, which overwhelm any buffering of juvenile survival achieved through climate-dependent selection.

Discussion

Even when multiple phenotypic traits are considered, evolutionary rescue fails under high-emissions climate warming, leaving climate mitigation as the dominant factor shaping future population trajectories in a long-lived seabird (Fig. 3). Under high-emission scenarios, the rate and magnitude of warming exceed the pace at which evolutionary change can influence population growth, such that adaptation alone—regardless of the trait under selection—does not prevent long-term population extinction. Climate mitigation consistently slows population decline and reduces extinction risk; however, sustained population recovery and evolutionary rescue occur only under low-emissions pathways and only when such climate mitigation is combined with climate-driven selection acting on traits that influence key demographic parameters (Fig. 4).

By considering multiple traits that influence different components of the life cycle, our analysis shows that adaptive potential depends not only on the strength of

selection acting through trait–vital rate relationships, but also on whether these relationships translate into gains in population growth across the life cycle. Our previous results showed that the contribution of traits to population growth rate reflects the interaction of two distinct sensitivities: the sensitivity of vital rates to trait variation, and the sensitivity of population growth to those vital rates (11). Traits can differ markedly in how strongly they influence demographic rates, and a trait with a strong effect on a given vital rate does not necessarily translate into a large change in population growth if that vital rate itself has limited demographic impact.

In our long-lived species, foraging activity strongly affects breeding success and exhibits the highest sensitivity of vital rates to trait variation, explaining why selection on activity can drive substantial population growth under historical environmental conditions. However, breeding success contributes relatively weakly to population growth in this long-lived species, and foraging activity is not directly influenced by sea surface temperature. In contrast, juvenile survival has a much stronger influence on population growth rate, even though its sensitivity to trait variation is more moderate. Because future, non-stationary climate projections primarily affect population growth through their impact on juvenile survival, evolutionary change in traits affecting breeding success does not buffer populations against climate-driven declines, which are instead dominated by changes in juvenile survival. Nevertheless, these traits still influence population trajectories by limiting recovery under high-emissions scenarios, even when climate-dependent selection partially improves juvenile survival (Fig. S3).

Within this framework, contrasts among traits illustrate how different adaptive pathways translate into population outcomes. Wing length, a morphological trait, influences population dynamics through its association with juvenile survival and recruitment, the demographic components that most strongly constrain population growth under climate change. As a result, when selection on wing length is directly coupled to climate change and mitigation slows the rate of warming, evolutionary rescue becomes possible in our simulations (Fig. 4). Notably, evolutionary rescue emerged even at moderate heritability values (Fig. S4), with populations rebounding to their initial size after an early decline for heritability as low as $h^2 = 0.3$. This value lies within empirically observed ranges for morphological traits in wild bird populations: in a comprehensive meta-analysis, the median heritability for morphological traits in birds is 0.31 (SE = 0.02) after accounting for publication year, estimation method, and uncertainty (24).

These results therefore identify a biologically plausible, yet conditional, pathway by which climate-driven selection could contribute to population persistence under strong climate mitigation. In the Southern Ocean, climate change is projected to alter atmospheric circulation, including strengthening and poleward shifts of the westerly wind systems (30). Such changes could modify the selective landscape for flight-related morphology, as soaring efficiency generally increases under stronger wind conditions (29). Under these circumstances, morphological variation associated with flight performance could confer differential survival advantages, particularly during the juvenile stage. However, any such advantage is likely to be constrained by ecological trade-offs. Larger body size or wing area may increase energetic demands, while warming ocean conditions are also expected to reduce prey availability in sub-Antarctic ecosystems (30). These counteracting forces could limit net fitness gains from morphological change, even under climate-driven selection. Consistent with this interpretation, evolutionary rescue in our simulations emerged only when climate-driven selection coincided with strong mitigation of greenhouse gas emissions, underscoring the narrow conditions under which adaptive responses could translate into population persistence.

In contrast to wing length, behavioral and phenological traits in our system exhibit limited evolutionary impact on population dynamics under future climate warming. Traits such as foraging activity, time on water, and return date primarily influence breeding success, a demographic component to which population growth is relatively insensitive in this long-lived species (11). However, these traits are inherently more dynamic than morphological traits, varying substantially among years and across individual lifetimes in response to environmental conditions and experience. As a result, they are more likely to respond through plastic or ontogenetic changes than through sustained evolutionary change (see Supporting Information).

Notably, although return date is a central adaptive trait in many short-lived taxa such as passerines (4, 31), its influence on population growth through climate change of black-browed albatross appears limited (11). This is consistent with global evidence that seabirds show little plasticity in reproductive timing, with no consistent advance in breeding dates despite warming ocean temperatures (32). Theory predicts that plastic responses in behavioral and phenological traits can buffer populations against short-term environmental deterioration, but may also weaken selection on heritable traits by reducing fitness variation among individuals, thereby slowing evolutionary responses (12, 33). We explicitly tested these hypotheses in supplementary analyses (Supporting Information) by allowing behavioral traits to vary plastically with climate and to improve with age and experience. While these mechanisms increased mean breeding success, they did not alter population trajectories or prevent extinction under future climate projections (Fig. S5, S6).

Conclusion

Our findings align with growing evidence from other taxa that natural selection alone may be insufficient to prevent biodiversity losses under rapid climate change. In reef-building corals, even under optimistic assumptions with high heritability and unbounded trait evolution, evolutionary adaptation only modestly delayed coral decline and failed to prevent extinction without strong climate mitigation (5). Our results in a long-lived seabird mirror this pattern: despite allowing for adaptation via multiple traits and and eco-evolutionary mechanisms, evolutionary responses alone were too slow or too weak to counteract climate-driven population decline. Similar conclusions have emerged in other species (4), where evolutionary adaptation may buy time to extinction, but is unlikely to prevent it without concurrent socio-economic

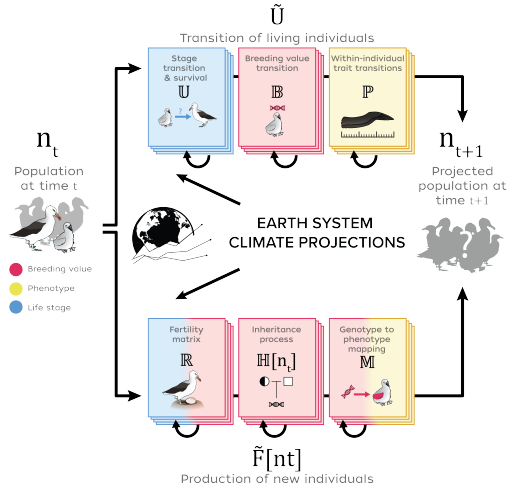

Fig. 1. Schematic of the hyperstate eco-evolutionary model. The population vector $\mathbf{n}_t$ is projected from time t to $t+1$ using a population matrix $\tilde{\mathbf{A}} = \tilde{\mathbf{U}} + \tilde{\mathbf{F}}$, constructed from modular sub-processes: $\mathbb{U}$ for stage transitions, $\mathbb{B}$ for breeding value dynamics, $\mathbb{P}$ for phenotype dynamics, $\mathbb{R}$ for fertility, $\mathbb{H}$ for inheritance of breeding values, and $\mathbb{M}$ for phenotypic assignment at birth. Permutation matrices reorder the state vector between sub-processes (shown as reshuffling arrows). Climate projections are incorporated through their effects on traits and vital rates, with population responses evaluated across large climate ensembles to account for internal climate variability.

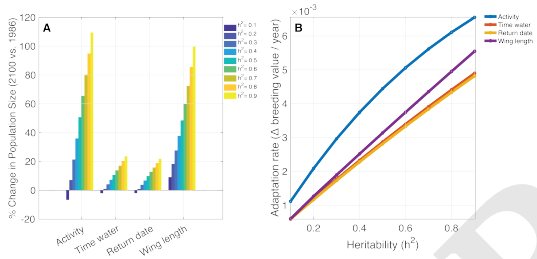

Fig. 2. Adaptive dynamics of black-browed albatross under constant climate conditions. (A) Projected percent change in total population size at the Kerguelen Islands by 2100 relative to initial abundance in 1986 across four phenotypes. Bars represent outcomes from eco-evolutionary simulations under a constant historical climate (average sea surface temperatures from 1986–2022). Colors indicate heritability values ranging from 0.1 to 0.9. (B) Adaptation rates, measured as the annual change in mean breeding value, predicted for each trait under constant historical sea surface temperatures as a function of heritability.

pathways for climate change mitigation that reduce the rate and magnitude of climate change.

Materials and Methods

We examined the eco-evolutionary responses of the long-lived black-browed albatross (*Thalassarche melanophris*) to climate change using long-term demographic, phenotypic, and environmental observations from the Kerguelen Islands (Supplementary Methods). We developed and parameterized a hyperstate eco-evolutionary matrix population model (9) using more than three decades of individual-based capture–mark–recapture data (11). The framework integrates demography, quantitative genetics, and trait variation within a unified population projection model (9) (Fig. 1). Following the hyperstate approach (34), individuals are classified simultaneously by demographic state i, breeding value j, and phenotype k. This structure allows the joint projection of population dynamics and adaptive evolution while explicitly tracking distributions of breeding values and phenotypes.

Under the infinitesimal model of quantitative genetics (35), phenotypic variance is partitioned into additive genetic and environmental components, and narrow-sense heritability is defined as the proportion of phenotypic variance explained by additive genetic variance:

$$V_P = V_A + V_E,$$
$$h^2 = \frac{V_A}{V_P}. \quad [1]$$

The population is represented by a hyperstate vector $\tilde{\mathbf{n}}_t$, which tracks abundance across all combinations of demographic states, breeding values, and phenotypes. Population dynamics are projected according to:

$$\tilde{\mathbf{n}}_{t+1} = \tilde{\mathbf{A}}\tilde{\mathbf{n}}_t,$$
$$\tilde{\mathbf{A}} = \tilde{\mathbf{U}} + \tilde{\mathbf{F}}. \quad [2]$$

The transition component $\tilde{\mathbf{U}}$ combines demographic transitions, breeding-value dynamics, and phenotype dynamics, whereas the reproductive component $\tilde{\mathbf{F}}$ combines fertility, inheritance of breeding values, and assignment of offspring phenotypes (Supplementary Methods). Demographic rates depend on both environmental conditions and individual trait values, allowing climate change to influence population dynamics directly and indirectly through natural selection. The framework accommodates both fixed traits and dynamic traits that vary through ontogeny or phenotypic plasticity (Supplementary Methods). Full mathematical derivations, inheritance functions, phenotype-assignment procedures, and block-matrix constructions are provided in the Supporting Information and in Van de Walle et al. (9).

Parameterizing eco-evolutionary models for long-lived species is inherently challenging because evolutionary responses unfold slowly relative to demographic change, while key genetic parameters are often poorly known. As in previous eco-evolutionary forecasting studies (5, 7), we therefore adopted a scenario-based approach to evaluate evolutionary potential and population responses under contrasting assumptions regarding inheritance, selection, and climate forcing. In this system, projected population decline is driven primarily by the effects of SST on juvenile survival. Previous analyses indicate that SST does not directly influence trait expression but instead affects populations through trait-dependent demographic rates (11). Consequently, evolutionary responses emerge indirectly through selection and are expected to unfold slowly in a species with a generation time of approximately 24 years (28).

Future environmental conditions are sea surface temperature (SST) trajectories derived from large ensembles of Earth System Model simulations (Supplementary Methods).

We evaluated three classes of scenarios:

1. **Historical environment.** Sea surface temperatures were held constant at the observed seasonal climatology, providing a stationary environmental benchmark for demographic and evolutionary dynamics.
2. **Climate change with uncertainty.** SST projections from individual ensemble members of the Community Earth System Model (CESM) were propagated through the eco-evolutionary model, allowing uncertainty associated with internal climate variability to be incorporated into population forecasts (Supplementary Fig. S7).
3. **Climate change with evolving selection pressures.** To investigate mechanisms of evolutionary rescue, we examined scenarios in which climate change alters the strength of selection acting on wing length through juvenile survival. Because the objective was to characterize the directional effects of climate-dependent selection, these analyses used ensemble-mean SST trajectories representing the forced climate signal. Additional analyses incorporating demographic and climate variability produced qualitatively similar eco-evolutionary outcomes but increased extinction risk by amplifying variation in vital rates (Supplementary Fig. S8).

Detailed descriptions of the study system, climate projections, hyperstate eco-evolutionary model, model parameterization, inheritance functions, phenotype assignment procedures, and additional analyses of phenotypic plasticity and ontogenetic change are provided in the Supporting Information.

Data, Materials, and Software Availability. All data and code required to reproduce the analyses are available through Figshare (https://doi.org/10.6084/m9.figshare.31095772). Upon publication, all materials will also be archived in a public GitHub repository (https://github.com/fledge-whoi), with Figshare serving as the permanent citable archive. Long-term demographic data were collected through monitoring programs conducted at Kerguelen Island and are available through the archived repository.

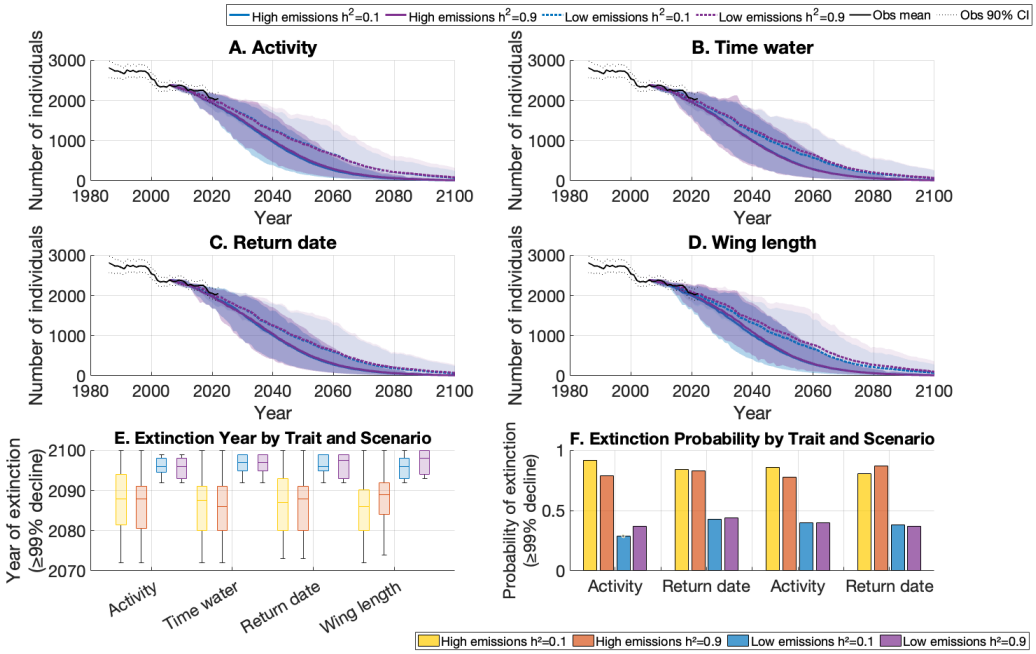

Fig. 3. Influence of heritability and climate on projected population dynamics of black-browed albatross. (A–D) Projected total population size from 2006 to 2100 for four phenotypes (activity, time on water, return date, and wing length) under a moderately high-emission pathway (SSP3-7.0) and a low-emission scenario consistent with the Paris Agreement, assuming heritability values of $h^2 = 0.1$ and 0.9. Solid lines denote SSP3-7.0 projections and dotted lines the Paris scenario. Colors indicate heritability, and shaded areas represent 90% confidence intervals incorporating demographic and climate uncertainty. Observed population estimates from an integral Bayesian population model are shown in black. (E) Time to extinction and (F) probability of extinction based on a 99% decline threshold. Boxes show interquartile ranges, medians, and 5th–95th percentiles.

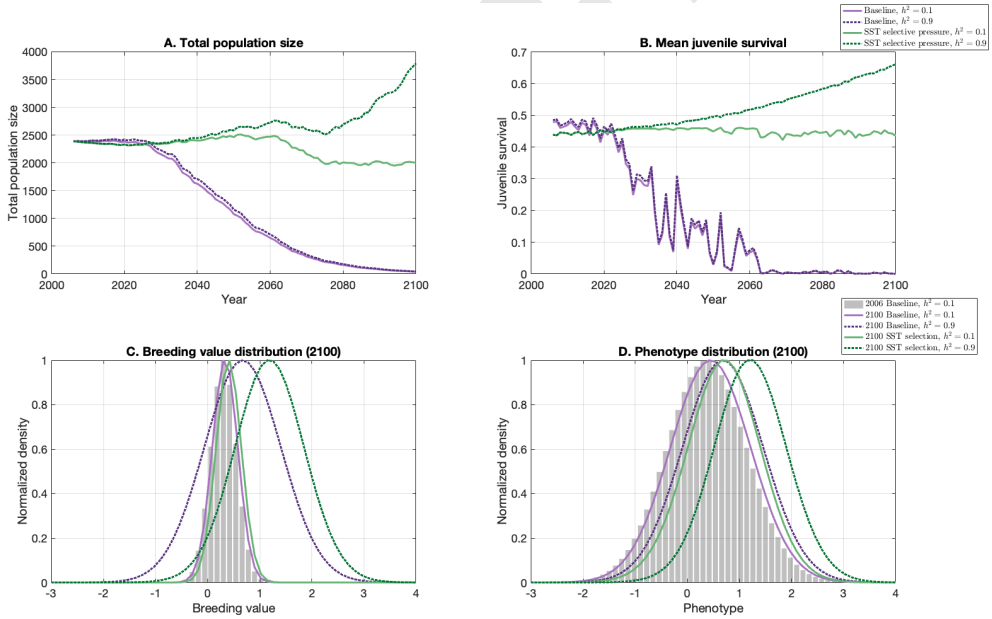

Fig. 4. Eco-evolutionary dynamics under low-emission climate projections with alternative selective pressures. Solid lines represent $h^2 = 0.1$ and dotted lines $h^2 = 0.9$. Wing length is either subject to increased selection under warmer sea surface temperatures (green) or assumed unaffected by climate change (purple). (A,B) Projected demographic trajectories from 2006 to 2100. (C,D) Initial (2006) and final (2100) distributions of breeding values and phenotypes. Initial trait distributions are shown only for the baseline scenario with $h^2 = 0.1$.

ACKNOWLEDGMENTS. We thank all field workers involved in long-term demographic studies on Kerguelen Island since 1960 for their invaluable contributions to data collection and Dominique Joubert for assistance with data management. Long-term demographic studies were supported by the Institut Polaire Français Paul-Émile Victor (IPEV project 109 ORNITHO2E, PI C. Barbraud), Terres Australes et Antarctiques Françaises, and Zone Atelier Antarctique et Terres Australes (LTSER France, CNRS). This study is part of the long-term Studies in Ecology and Evolution (SEE-Life) program of the CNRS. This work was supported by the National Science Foundation (ORCC grant 2222057). The authors used artificial intelligence–assisted tools to support language editing and improve clarity of presentation; all scientific content, analyses, and conclusions were developed by the authors.

1. R Gomulkiewicz, RD Holt, When does evolution by natural selection prevent extinction? *Evolution* **49**, 201–207 (1995).
2. A Gonzalez, O Ronce, R Ferriere, ME Hochberg, Evolutionary rescue: an emerging focus at the intersection between ecology and evolution. *Philos. Transactions Royal Soc. B: Biol. Sci.* **368**, 20120404 (2013).
3. MC Urban, et al., When and how can we predict adaptive responses to climate change? *Evol. Lett.* **8**, 172–187 (2024).
4. EG Simmonds, EF Cole, BC Sheldon, T Coulson, Phenological asynchrony: A ticking time-bomb for seemingly stable populations? *Ecol. Lett.* **23**, 1766–1775 (2020).
5. L Lachs, et al., Natural selection could determine whether acropora corals persist under expected climate change. *Science* **386**, 1289–1294 (2024).
6. T Coulson, T Potter, A Felmy, Predicting evolution over multiple generations in deteriorating environments using evolutionarily explicit integral projection models. *Evol. Appl.* **14**, 2490–2501 (2021).
7. TJ Clark-Wolf, PD Boersma, F Plard, GA Rebstock, B Abrahms, Increasing environmental variability inhibits evolutionary rescue in a long-lived vertebrate. *Proc. Natl. Acad. Sci.* **121**, e2406314121 (2024).
8. S Jenouvrier, et al., Living with uncertainty: Using multi-model large ensembles to assess emperor penguin extinction risk for the iucn red list. *Biol. Conserv.* (2025).
9. JV de Walle, J Garnier, T Bonnet, S Jenouvrier, Toward a unified approach to modeling adaptation among demographers and evolutionary ecologists. *Methods Ecol. Evol.* (2025).
10. C Deser, A Phillips, V Bourdette, H Teng, Uncertainty in climate change projections: The role of internal variability. *Clim. Dyn.* **38**, 527–546 (2012).
11. S Jenouvrier, et al., Climate change and functional traits affect population dynamics of a long-lived seabird. *J. Anim. Ecol.* **87**, 906–920 (2018).
12. LM Chevin, R Lande, GM Mace, Adaptation, plasticity, and extinction in a changing environment: towards a predictive theory. *PLoS biology* **8**, e1000357 (2010).
13. T Coulson, et al., Modeling Adaptive and Nonadaptive Responses of Populations to Environmental Change. *The Am. Nat.* **190** (2017).
14. MC Urban, Accelerating extinction risk from climate change. *Science* **348**, 571–573 (2015).
15. L Chevin, J Bridle, Impacts of limits to adaptation on population and community persistence in a changing environment. *Philos. Transactions Royal Soc. B* **380**, 20230322 (2025).
16. T Bonnet, et al., Genetic variance in fitness indicates rapid contemporary adaptive evolution in wild animals. *Science* **376**, 1012–1016 (2022).
17. H Kokko, The stagnation paradox: the ever-improving but (more or less) stationary population fitness. *Proc. Royal Soc. B* **288**, 20212145 (2021).
18. JM Henshaw, MB Morrissey, AG Jones, Quantifying the causal pathways contributing to natural selection. *Evolution* **74**, 2560–2574 (2020).
19. O Cotto, L Sandell, L Chevin, O Ronce, Maladaptive shifts in life history in a changing environment. *The Am. Nat.* **194**, 558–573 (2019).
20. T Reed, V Grøtan, S Jenouvrier, BE Sæther, M Visser, Population growth in a wild bird is buffered against negative effects of phenological mismatch. *Science* **340**, 488–491 (2013).
21. MC Dietze, *Ecological forecasting*. (Princeton University Press), (2017).
22. S Jenouvrier, Impacts of climate change on avian populations. *Glob. Chang. Biol.* **19**, 2036–2057 (2013).
23. D Houle, Comparing evolvability and variability of quantitative traits. *Genetics* **130**, 195–204 (1992).
24. E Postma, Four decades of estimating heritabilities in wild vertebrate populations: improved methods, more data, better estimates? in *Quantitative genetics in the wild*, eds. A Charmentier, D Garant, LEB Kruuk. (Oxford University Press, Oxford), 1st edition, pp. 16–33 (2014).
25. KB Rodgers, et al., Ubiquity of human-induced changes in climate variability. *Earth Syst. Dyn.* **12**, 1393–1411 (2021).
26. BM Sanderson, et al., Community climate simulations to assess avoided impacts in 1.5 and 2 c futures. *Earth Syst. Dyn.* **8**, 827–847 (2017).
27. NA Dochtermann, T Schwab, M Anderson Berdal, J Dalos, R Royauté, The heritability of behavior: a meta-analysis. *J. Hered.* **110**, 403–410 (2019).
28. JP Bird, et al., Generation lengths of the world's birds and their implications for extinction risk. *Conserv. Biol.* **34**, 1252–1261 (2020).
29. H Weimerskirch, M Louzao, S de Grissac, K Delord, Changes in wind pattern alter albatross distribution and life-history traits. *science* **335**, 211–214 (2012).
30. AJ Constable, et al., Climate change and southern ocean ecosystems i: how changes in physical habitats directly affect marine biota. *Glob. change biology* **20**, 3004–3025 (2014).
31. A Charmantier, et al., Adaptive phenotypic plasticity in response to climate change in a wild bird population. *science* **320**, 800–803 (2008).
32. K Keogan, et al., Global phenological insensitivity to shifting ocean temperatures among seabirds. *Nat. Clim. Chang.* **8**, 313–318 (2018).
33. RJ Fox, JM Donelson, C Schunter, T Ravasi, JD Gaitán-Espitia, Beyond buying time: the role of plasticity in phenotypic adaptation to rapid environmental change. *Philos. Transactions Royal Soc. B: Biol. Sci.* **374**, 20180174 (2019).
34. G Roth, H Caswell, Hyperstate matrix models: Extending demographic state spaces to higher dimensions. *Methods Ecol. Evol.* **7**, 1438–1450 (2016).
35. LE Kruuk, A Charmantier, D Garant, The study of quantitative genetics in wild populations. *Quant. genetics wild* pp. 1–15 (2014).

PNAS

Supporting Information for

Climate mitigation contributes more to population persistence than evolutionary adaptation in a long-lived seabird

Jenouvrier, Garnier, Holland, van de Walle, Patrick, Bonnet, Delord, Ventura, Barbraud, and Weimerskirch

Stéphanie Jenouvrier E-mail: sjenouvrier@whoi.edu

This PDF file includes:

Supporting Information Text

This Supporting Information provides additional methodological details, analyses, and figures supporting the eco-evolutionary forecasts presented in the main manuscript. First, we present an expanded description of the study system, climate projections, and hyperstate eco-evolutionary population model, including the full mathematical formulation of demographic, inheritance, and phenotype-assignment processes. These sections provide the detailed derivations underlying the concise description presented in the main text.

We also include ten supplementary figures (Figs. S1–S10). These figures provide additional information on model validation, climate projections, uncertainty propagation, alternative selective-pressure scenarios, and the eco-evolutionary consequences of varying heritability. Several figures illustrate the effects of demographic and climatic uncertainty on projected population trajectories and evolutionary outcomes.

Finally, we examine a key assumption of the main analyses: that phenotypic traits remain fixed throughout life. Because available longitudinal data are insufficient to robustly estimate age-dependent or environmentally driven trait dynamics, the main analyses assume fixed phenotypes. In the section *Exploring Phenotypic Plasticity and Ontogenetic Change*, we relax this assumption and investigate two biologically motivated scenarios in which foraging traits vary through time. These analyses explore whether optimistic levels of phenotypic plasticity or age-related improvement could substantially alter conclusions regarding population persistence and evolutionary rescue.

Methods

Study System and Observed Population Trajectories . Black-browed albatross, is a long-lived, colonial Procellariiform seabird with annual breeding and a circumpolar distribution in the Southern Ocean. Our analyses are based on a multi-decadal demographic dataset from the Kerguelen Islands (49°41S, 70°14E). During the breeding season (October–April), birds forage in sub-Antarctic waters along the northeastern Kerguelen shelf, and migrate to Tasmanian waters during the non-breeding season. Diet is dominated by fish.

Standardized individual-based monitoring has been conducted at Kerguelen since 1987, comprising approximately 6,500 marked individuals. This long-term capture–mark–recapture program includes annual monitoring of breeding adults and ringing of all chicks prior to fledging, along with standardized measurements of body mass and wing length.

In addition to demographic and morphological data, we considered behavioral foraging and phenological traits, including activity, time spent on the water, and return date to the breeding colony(1). Behavioral and phenological traits were quantified using geolocator (GLS) deployments on breeding adults (2), which provide detailed trait distributions and estimates of phenotypic variance (V_P).

The GLS dataset spans eight non-breeding seasons (2006–2013) and includes repeated measurements for individual birds (64–86 individuals and 118–146 trips; (2)), but typically over only one to a few years per individual. Although these data offer a unique window into individual-level behavioral variation, their limited temporal and environmental coverage precludes robust estimation of age- or climate-dependent trait dynamics across the full life cycle. Given these limitations, the core analyses in the main text assume that phenotypic traits are fixed within individuals. We subsequently relax this assumption in supplementary analyses (Supplementary Indormation) to qualitatively explore the potential effects of phenotypic plasticity and ontogenetic change on eco-evolutionary population dynamics (Fig S9, S10).

Demographic rates and traits depend on SST experienced in distinct foraging regions and seasons of the life cycle(1, 2). Winter SST (Fig S7 A) mainly affects juvenile survival, wwhereas SST during the pre-breeding, wintering, and breeding seasons of adults (Fig S7 B, C) shapes adult foraging activity, migratory timing, and reproductive success

Observed population trajectories of black-browed albatrosses at Kerguelen (Fig S1) were estimated using age- and stage-structured Bayesian integrated population models (IPMs) (3) that jointly analyse capture–mark–recapture data, colony counts, and breeding productivity accounting for observation error and unobserved life stages, particularly juveniles and immatures that remain at sea for several years. The model is female-based, assume equal sex ratios at birth and strong natal philopatry, and incorporate age-specific recruitment and breeding transitions across the full life cycle. Population counts are modelled using a state-space formulation, survival and breeding states using a multi-event framework, and productivity using binomial regressions. These model outputs provide robust estimates of population trajectories over the observed period, which we use both to evaluate model hindcasts and to parameterize and benchmark the initial population of our eco-evolutionary projections under future climate scenarios.

Earth System Model Simulations. We used climate projections from two experiments based on the Community Earth System Model (CESM) framework to evaluate eco-evolutionary responses under contrasting climate scenarios: a high-emissions pathway and a stabilization scenario consistent with the Paris Agreement (low-emissions pathway). CESM is a state-of-the-art fully coupled Earth system model that has been widely used and evaluated in both CMIP5 and CMIP6. While multi-model ensembles offer insight into structural model uncertainty, our focus here is on forecasts that explicitly account for internal climate variability. We therefore rely on large ensemble simulations from a single model family (CESM1 and CESM2), which enable us to isolate the forced climate signal from natural variability and to propagate ensemble uncertainty through eco-evolutionary population projections.

The stabilization scenario is based on the CESM1-CAM5 ensemble developed by (4), using the 2.0°NE (never-exceed) pathway. This scenario was specifically designed to stabilize global mean temperature at 2°C above preindustrial levels by 2100. Emissions follow RCP8.5 until 2017 and then rapidly decline, reaching net-zero by 2078 and incorporating moderate negative

emissions thereafter. Simulations were performed with CESM1.1.1 (5), which includes coupled components for atmosphere (CAM5), ocean (POP2), land (CLM4), and sea ice (CICE4), all at a nominal ∼1° resolution. The ensemble consists of 11 members that branch from a historical simulation in 2006. Variations across the ensemble members allow us to quantify internal climate variability.

The high-emissions scenario comes from the CESM2 Large Ensemble (CESM2-LE; (6)), which follows the upper-middle SSP3-7.0 pathway. CESM2 includes updated model components—CAM6 (atmosphere), CLM5 (land), POP2 (ocean), and CICE5.1.2 (sea ice)—run at a nominal 1° resolution (7). The ensemble includes 50 members initialized from perturbed states of a preindustrial control run starting in 1850. All members are subjected to the same historical (1850–2014) and future (2015–2100) forcings under CMIP6 protocols (8). This design enables robust quantification of both externally forced responses and internal variability relevant to ecological forecasting.

Each CESM member represents an equally plausible realization of climate evolution, allowing the ensemble mean to isolate the externally forced signal, while the spread across members captures internal climate variability (9). For climate-driven scenarios comparison (sections and Supplementary Information), we analyze ensemble means. For population projections that incorporate uncertainty in climate drivers, we propagate each individual ensemble member through the eco-evolutionary model.

Sea surface temperature (SST) projections from both CESM1 and CESM2 experiments closely match observed seasonal SST patterns within the foraging range of black-browed albatrosses (Fig. S7). Across all stages of the life cycle—including the breeding season for adults and wintering periods of both adults and juveniles—modeled SSTs align well with satellite-based interannual variability. This agreement supports the use of these simulations for forecasting environmentally driven demographic responses in this species.

Hyperstate Matrix Eco-Evolutionary Population Model. We developed a hyperstate eco-evolutionary matrix population model that integrates multiple individual-level traits and demographic states (10) (Fig. **??**). The hyperstate matrix framework (11) classifies individuals along three key dimensions: (1) demographic state i (e.g., age and breeding stage), (2) breeding value j, and (3) phenotype k (e.g., foraging behaviors, return date or wing length). This structure enables us to simultaneously track both heritable and phenotypic variations within the population and to model their joint effects on demography and evolution.

Under the classical infinitesimal model of quantitative genetics, an individual's phenotype is modeled as the sum of an additive genetic component—termed the breeding value—and an environmental component, with the genetic contribution of offspring normally distributed around the mid-parental mean and with variance independent of parental traits (12). The change in the mean breeding value over time defines the genetic evolution of the trait. The variance of breeding values is the additive genetic variance, denoted V_{A}, while the variance of environmental deviations is the environmental variance, V_{E}. These together constitute the total phenotypic variance V_{P}:

$$V_{\mathrm{P}} = V_{\mathrm{A}} + V_{\mathrm{E}}. \quad [1]$$

Narrow-sense heritability, denoted h^2, quantifies the proportion of phenotypic variance explained by additive genetic factors:

$$h^2 = \frac{V_{\mathrm{A}}}{V_{\mathrm{P}}}. \quad [2]$$

The total population size at time t, denoted N_t, is obtained by summing over all individuals described by the state vector $\tilde{\mathbf{n}}_t$, which tracks the number of individuals across all combinations of demographic state, breeding value, and phenotype class. The population is projected to time $t+1$ using the matrix $\tilde{\mathbf{A}}$:

$$\tilde{\mathbf{n}}_{t+1} = \tilde{\mathbf{A}}\tilde{\mathbf{n}}_t. \quad [3]$$

Although the model tracks only females explicitly, a two-sex formulation incorporates the distribution of male breeding values for inheritance, assuming a parallel population structure in males and females.

The projection matrix $\tilde{\mathbf{A}}$ can be decomposed into a survival-transition component $\tilde{\mathbf{U}}$ and a reproduction component $\tilde{\mathbf{F}}$ (Fig. **??**). These components, in turn, are constructed from sub-processes operating within each dimension. Transition and reproduction steps use permutation matrices $\mathbf{K}_{s,b}$ and $\mathbf{K}_{b,p}$ to reorder the state vector between sub-processes (13).

The transition matrix is given by:

$$\tilde{\mathbf{U}} = (\mathbf{K}_{b,p}\mathbf{K}_{s,b})^{\mathrm{T}}\mathbb{P}\mathbf{K}_{b,p}\mathbb{B}\mathbf{K}_{s,b}\mathbb{U} \quad [4]$$

where $\mathbb{U}$ represents transitions between states within each breeding value and phenotype class, $\mathbb{B}$ represents breeding value transitions within each state and phenotype, and $\mathbb{P}$ represents phenotype transitions within each state and breeding value.

The reproduction matrix is defined as:

$$\tilde{\mathbf{F}}[\tilde{\mathbf{n}}_t] = (\mathbf{K}_{b,p}\mathbf{K}_{s,b})^{\mathrm{T}}\,\mathbb{M}\,\mathbf{K}_{b,p}\,\mathbb{H}[\tilde{\mathbf{n}}_t]\,\mathbf{K}_{s,b}\,\mathbb{R}. \quad [5]$$

where $\mathbb{R}$ contains stage-specific fertility rates, $\mathbb{H}$ models the inheritance of breeding values, and $\mathbb{M}$ determines phenotypic assignment of offspring based on breeding value and environmental variance.

Each of the block matrices $\mathbb{U}$, $\mathbb{B}$, $\mathbb{P}$, $\mathbb{R}$, $\mathbb{H}$, and $\mathbb{M}$ is composed of smaller matrices placed on the diagonal. For example, the block-diagonal matrix $\mathbb{U}$ is defined as:

$$\mathbb{U} = \begin{pmatrix} \mathbf{U}_{11} & \mathbf{0} & \cdots & \mathbf{0} \\ \mathbf{0} & \mathbf{U}_{21} & \cdots & \mathbf{0} \\ \vdots & \vdots & \ddots & \vdots \\ \mathbf{0} & \mathbf{0} & \cdots & \mathbf{U}_{bp} \end{pmatrix}. \quad [6]$$

with similar block-diagonal constructions for the matrices $\mathbb{R}$, $\mathbb{B}$, $\mathbb{H}$, $\mathbb{P}$, and $\mathbb{M}$.

$\mathbb{U}$ is composed of matrices $\mathbf{U}_{jk}$ and is parameterized using stage transition rates such as survival, recruitment and breeding probabilities, estimated from individual capture–mark–recapture (CMR) data (1) (Fig. **??**).

$\mathbb{B}$ contains identity matrices $\mathbf{B}_{ik}$, since breeding values are assumed fixed at birth.

$\mathbb{P}$ includes phenotype transition matrices $\mathbf{P}_{ij}$, which are identity matrices for traits fixed across life, or age- or environment-dependent for plastic or ontogenetic traits (Supplementary Information , Fig. S9, S10).

$\mathbb{R}$ is composed of matrices $\mathbf{R}_{jk}$ that represent state-specific fertility rates estimated from individual CMR data (1) .

$\mathbb{H}$ models inheritance. Offspring breeding values are drawn from a normal distribution centered on the mid-parent mean $(x_{jf} + x_{jm})/2$, with variance $V_\mathrm{A}/2$. Values of V_A are obtained from equation 2 and the observed phenotypic variance V_P.

$\mathbb{M}$ assigns offspring to phenotypic classes based on their breeding value and environmental variance. Given the heritability, the environmental variance is calculated as:

$$V_\mathrm{E} = V_\mathrm{P}(1 - h^2). \quad [7]$$

From the projected population $\tilde{\mathbf{n}}_t$ and the projection matrix $\tilde{\mathbf{A}}$, we derive key demographic and evolutionary outcomes. These include population growth rate, total population size, as well as time trends in mean vital rates such as survival and reproduction. Evolutionary outcomes include the rate of adaptation, measured via changes in mean breeding and phenotypic values, and the temporal distribution of phenotypic and breeding classes.

Parametrization of the Hyperstate Matrix Eco-Evolutionary Population Model. We parameterized the hyperstate eco-evolutionary matrix population model using long-term individual-based data from a capture–mark–recapture (CMR) study of black-browed albatrosses breeding at Kerguelen Island, spanning more than three decades (1) (section). Demographic rates, including survival, recruitment, breeding probability, and breeding success across life-history states, were estimated from multi-event CMR models developed in previous studies (1). Relationships linking climate variability and individual traits to demographic rates were derived also from (1) that quantified how sea surface temperature influences functional traits—such as wing length at fledging, foraging behavior, and phenology—and how these traits, in turn, affect vital rates across the full life cycle. These empirically estimated climate–trait–demography linkages provide the basis for parameterizing trait-dependent transitions and reproduction within the hyperstate framework. Specifically, sea surface temperature, along with the assigned phenotype classes, determine the values of demographic rates used to parameterize the survival and reproduction matrices $\mathbb{U}$ and $\mathbb{R}$.

Although the dataset spans more than three decades, the long generation time of this species (∼24 years (14)) results in a relatively shallow demographic pedigree, precluding robust estimation of trait heritability from the population data. Therefore, we explored a range of heritability values to bracket plausible evolutionary responses under future climate change following previous approaches (15, 16). In particular, in our future projections, we focused on two contrasting scenarios, $h^2 = 0.1$ and $h^2 = 0.9$, representing weak and near-maximal contributions of additive genetic variance to phenotypic variation, respectively. The high-heritability case provides an upper bound on adaptive potential, analogous to a theoretical best-case scenario in which evolutionary responses are maximized, allowing us to test whether even optimistic assumptions about inheritance are sufficient to buffer climate-driven population decline. The low-heritability case reflects more conservative expectations for complex behavioral, phenological, or life-history traits in long-lived species. To assess robustness, we explored a wider range of heritability values in additional scenarios, confirming that the qualitative conclusions are not sensitive to intermediate values of h^2 (Fig. S4).

For a given value of heritability and the observed variance in the phenotypic distribution V_P, we derive the corresponding additive genetic variance V_A and environmental variance V_E (equation 2). These quantities are then used to parameterize the inheritance matrix $\mathbb{H}$ and the phenotypic assignment matrix $\mathbb{M}$, respectively.

Specifically, the probability that a female with breeding value class j_f mates with a male in class j_m and produces offspring with breeding value class j is given by:

$$G_{V_\mathrm{A}}\left(x_j - \frac{x_{j_f} + x_{j_m}}{2}\right)\delta_{j_m}(\mathbb{R}\tilde{\mathbf{n}}_t), \quad [8]$$

where G_{V_A} is a Gaussian distribution with mean 0 and variance $V_\mathrm{A}/2$, normalized so that the total probability across breeding values j equals 1 for any pair of parental breeding values j_f and j_m. The function $\delta_{j_m}(\mathbb{R}\tilde{\mathbf{n}})$ denotes the frequency of reproductive males in class j_m within the population. Due to limited data on individual sex in black-browed albatrosses, we assume an even sex ratio and similar selective pressures across sexes. Under this assumption, the frequency of reproductive males is equivalent to that of reproductive females and is computed as:

$$\delta_{j_m}(\mathbb{R}\mathbf{n}) = \frac{\sum_{i=1}^{s}\sum_{k=1}^{p} F_{j_m,k} n_{i,j_m,k}}{\sum_{i=1}^{s}\sum_{j=1}^{b}\sum_{k=1}^{p} F_{j,k} n_{i,j,k}} \quad [9]$$

where $F_{j,k}$ denotes the fertility rate for individuals in breeding value class j and phenotype class k, and $n_{i,j,k}$ is the number of individuals in demographic state i, breeding value class j, and phenotype class k.

The inheritance matrix $\mathbf{H}_{i,k}[\mathbf{n}]$ for demographic stage i and phenotype class k specifies the probability that a mother in breeding value class j_f produces offspring in breeding value class j, and is defined as:

$$(\mathbf{H}_{i,k}[\mathbf{n}])_{j,j_f} = \sum_{j_m=1}^{b} G_{V_\mathrm{A}}\left(x_j - \frac{x_{j_f} + x_{j_m}}{2}\right)\delta_{j_m}(\mathbb{R}\mathbf{n}). \quad [10]$$

The phenotype assignment matrix $\mathbf{M}_{i,j}$ (of dimension $p \times p$) gives the probability that an offspring with breeding value x_j is assigned to phenotype class k at birth. This assignment is based solely on the offspring's breeding value and is independent of the parental phenotype. The probability that an offspring with breeding value x_j expresses phenotype z_k is:

$$G_{V_\mathrm{E}}(z_k - x_j), \quad [11]$$

where G_{V_E} is a Gaussian distribution with mean 0 and variance $V_\mathrm{E} = (1 - h^2)V_\mathrm{P}$. The distribution is normalized so that its sum over phenotype classes k equals 1 for each breeding value j. Accordingly, the matrix $\mathbf{M}_{i,j}$ is given by:

$$\mathbf{M}_{i,j} = \left(G_{V_\mathrm{E}}(z_k - x_j)\right)_{k=1,\ldots,p}. \quad [12]$$

Scenarios of Climate-dependent Selection on Juvenile Survival. To explore mechanisms that could buffer population decline, we implemented an alternative scenarios of selective pressure on juvenile survival. We assumed that environmental change itself alters the strength of selection: under this climate-dependent selection scenario, survival advantages associated with longer wings increase as SST rises. This reflects a plausible ecological mechanism in a warming Southern Ocean, where strengthening and poleward-shifting westerly winds are expected to favor individuals with larger wing spans due to improved soaring efficiency (17, 18).

First-year survival (θ) is modeled with a logistic function of sea surface temperature (SST) and wing length. We examined two formulations (Fig. S2):

- **Baseline scenario:** Survival depends additively on SST and wing length, matching the empirically estimated relationship (1) (Fig. S2**A**):
$$\theta = \mathrm{logit}^{-1}\left(-0.23 - 0.24\,\mathrm{SST} - 0.32\,\mathrm{SST}^2 + 0.368\,\mathrm{WING}\right). \quad [13]$$
- **Climate-dependent selection:** The strength of selection varies with SST, such that the survival advantage of longer wings increases as SST rises (Fig. S2**B**). This introduces an interaction between wing length and SST:
$$\theta = \mathrm{logit}^{-1}\left(-0.23 - 0.24\,\mathrm{SST} - 0.32\,\mathrm{SST}^2 + 0.368\,\mathrm{WING}\cdot\mathrm{SST}\right). \quad [14]$$

Supplementary Figures

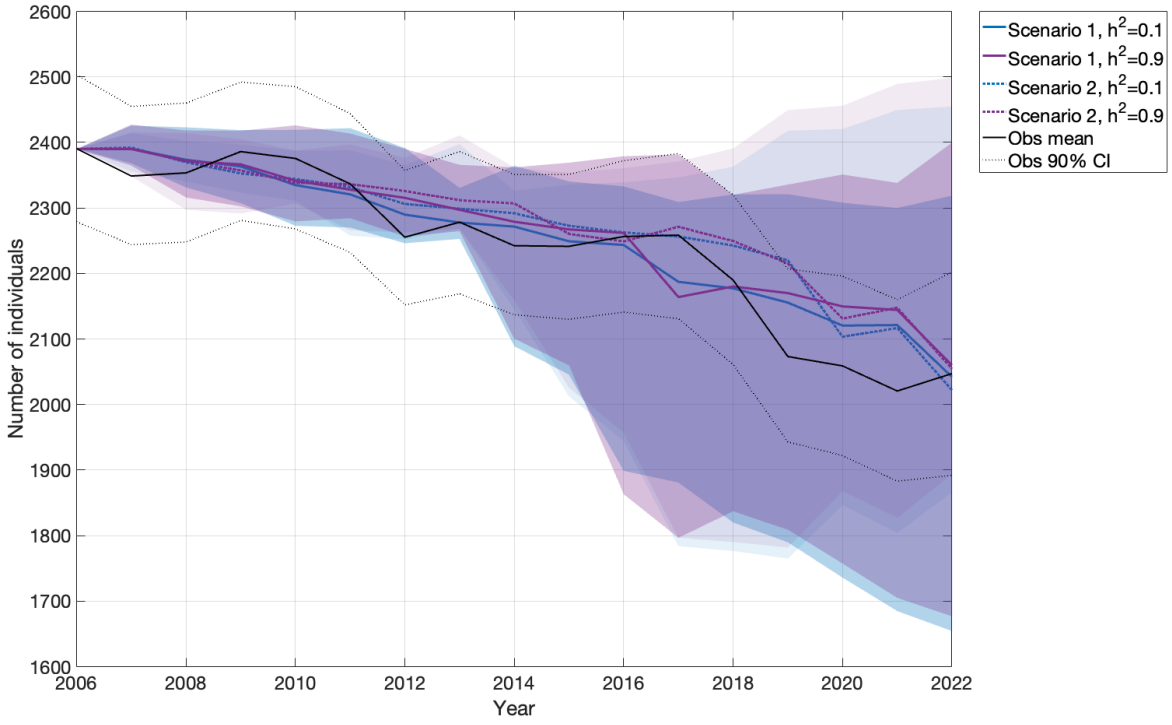

Fig. S1. Supplementary Figure S1. Hindcast of population trajectories during the observed period. Zoom of Fig. ?? in the main manuscript over the observed period (2006–2022), shown for the Activity trait. Lines indicate median projected population size and shaded areas denote 90% uncertainty envelopes for each climate pathway and heritability value, overlaid with the observed population mean (solid black line) and 90% confidence interval (dotted black lines). Hindcasts correspond to retrospective projections initialized with observed demographic states and evaluated against empirical data. The close agreement between hindcast projections and observations supports the model's ability to reproduce recent population dynamics. The same qualitative pattern is observed across all traits shown in Fig. 3; only Activity is shown here for clarity.

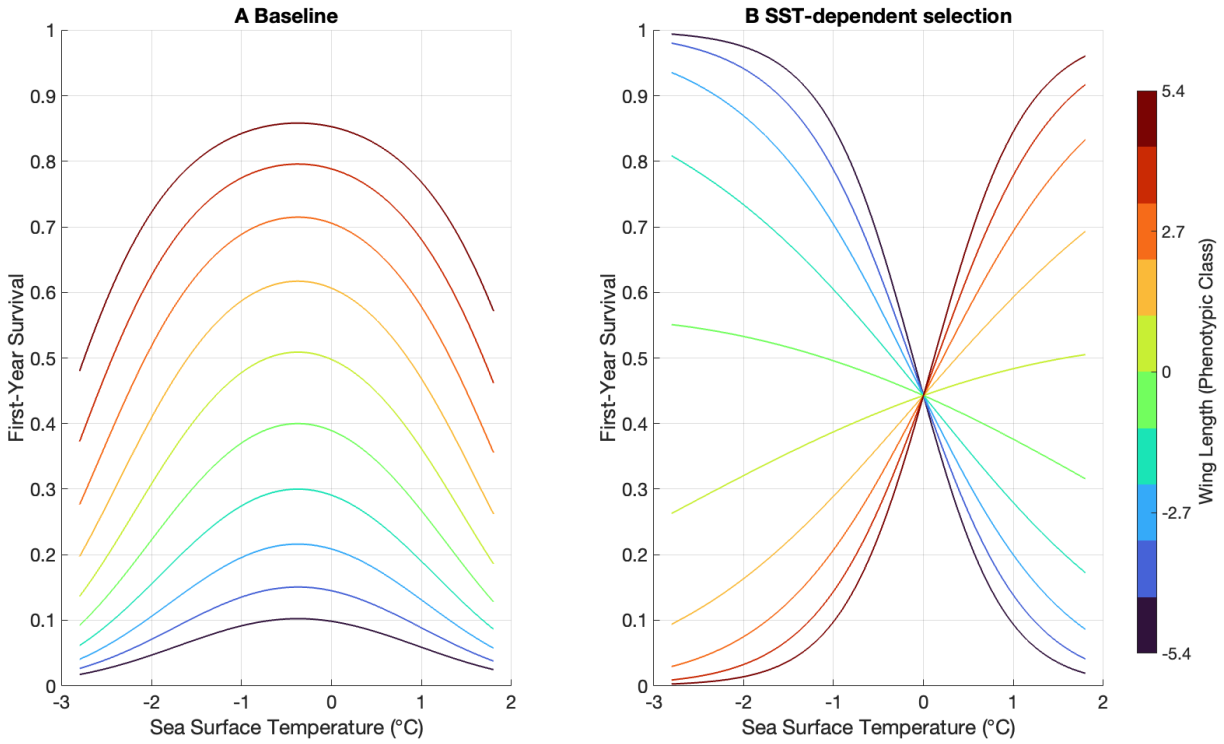

Fig. S2. Supplementary Figure S2. Sea surface temperature and wing length determine juvenile survival under two scenarios. Each panel shows predicted first-year survival as a function of sea surface temperature (SST) for individuals differing in wing length (color). Here wing length is binned into 10 phenotypic classes, with color indicating increasing length (blue to red), but our model includes 100 phenotypic classes. (A) Baseline scenario assumes SST and wing length influence survival independently as estimated empirically (1). (B) In the SST-dependent selection scenario, the survival advantage of longer wings increases with warming, while individuals with shorter wings experience even lower survival.

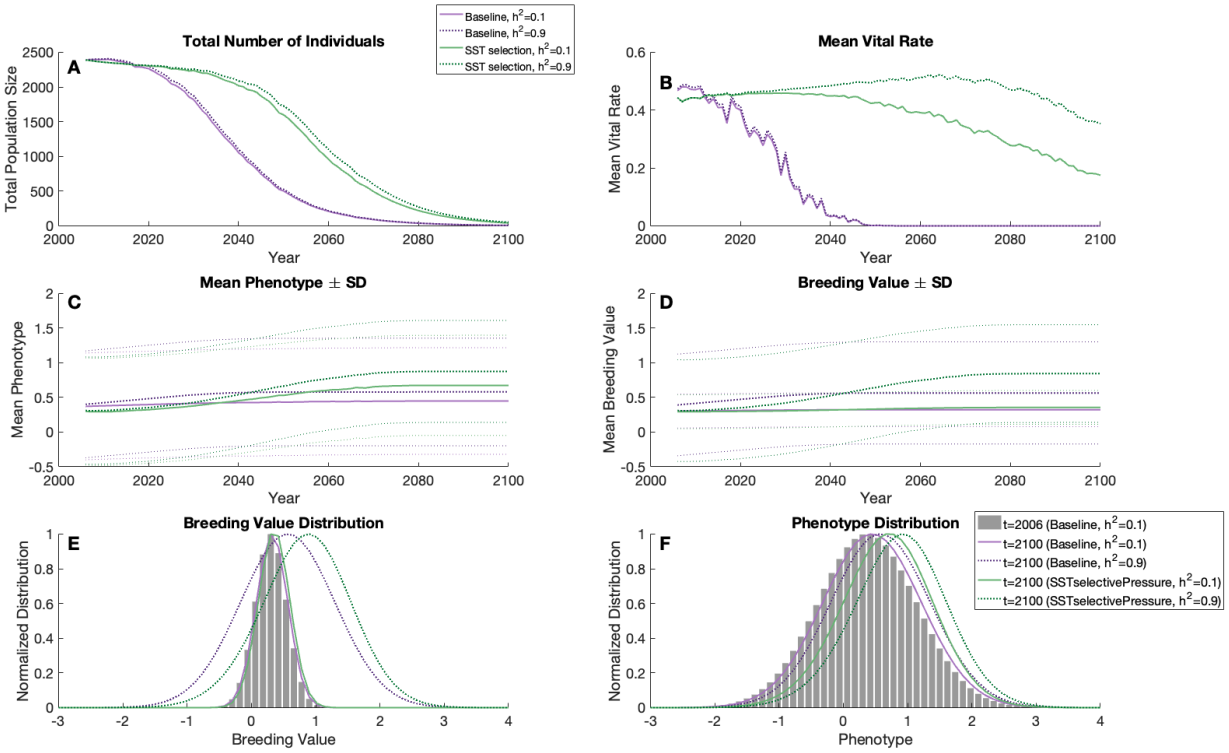

Fig. S3. Supplementary Figure S3. Eco-evolutionary response of black-browed albatross under alternative selective pressures under high-emissions climate projections. We present two scenarios of selection on wing length, a trait measured at fledging that influences juvenile survival and recruitment. In the baseline scenario, juvenile survival is a function of both sea surface temperature (SST) and wing length, but selection on wing length is independent of climate (i.e., the effect of wing length on survival remains constant across SST conditions). In the SST-dependent selection scenario, SST directly modifies the strength of selection on wing length: the survival advantage of longer wings increases under warmer conditions, thereby intensifying trait-based selection as the climate warms. (A) Total population size, (B) mean vital rate (i.e., breeding success), (C) mean phenotype $\pm$ 1 SD (i.e., Activity), and (D) mean breeding value $\pm$ 1 SD from 2006 to 2100. (E,F) Final (2100) and initial (2006) distributions of breeding value and phenotype. Solid lines represent $h^2 = 0.1$, dotted lines $h^2 = 0.9$. Colors distinguish scenarios: purple = baseline and green = SST-dependent selection. Initial distributions (grey bars) are shown only for the baseline scenario with $h^2 = 0.1$.

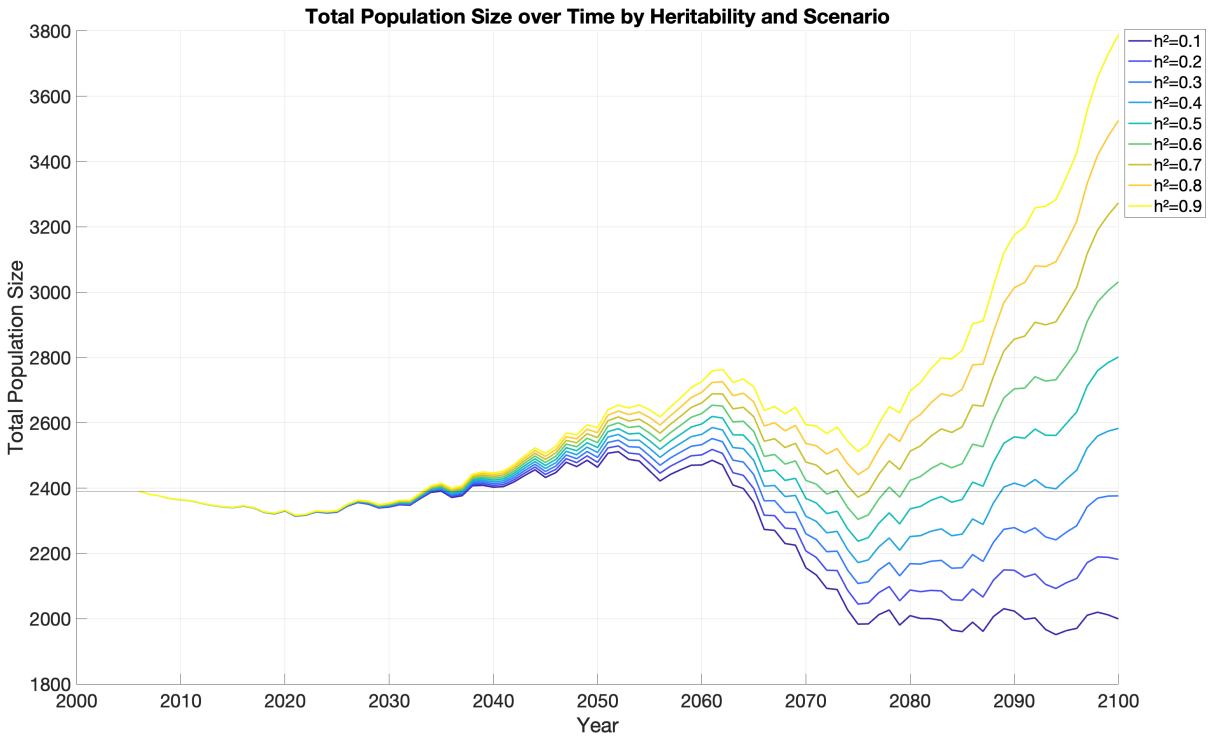

Fig. S4. Supplementary Figure S4. Eco-evolutionary dynamics of black-browed albatross under low-emissions climate projections with sea surface temperature-dependent selection. Total population size from 2006 to 2100 across a range of heritability values (h^2), showing that evolutionary rescue occurs above a threshold near $h^2 = 0.3$, a realistic estimate for morphological traits (19). Colored lines represent increasing heritability from low (blue) to high (yellow). The horizontal black line indicates the initial population size in 2006 for reference.

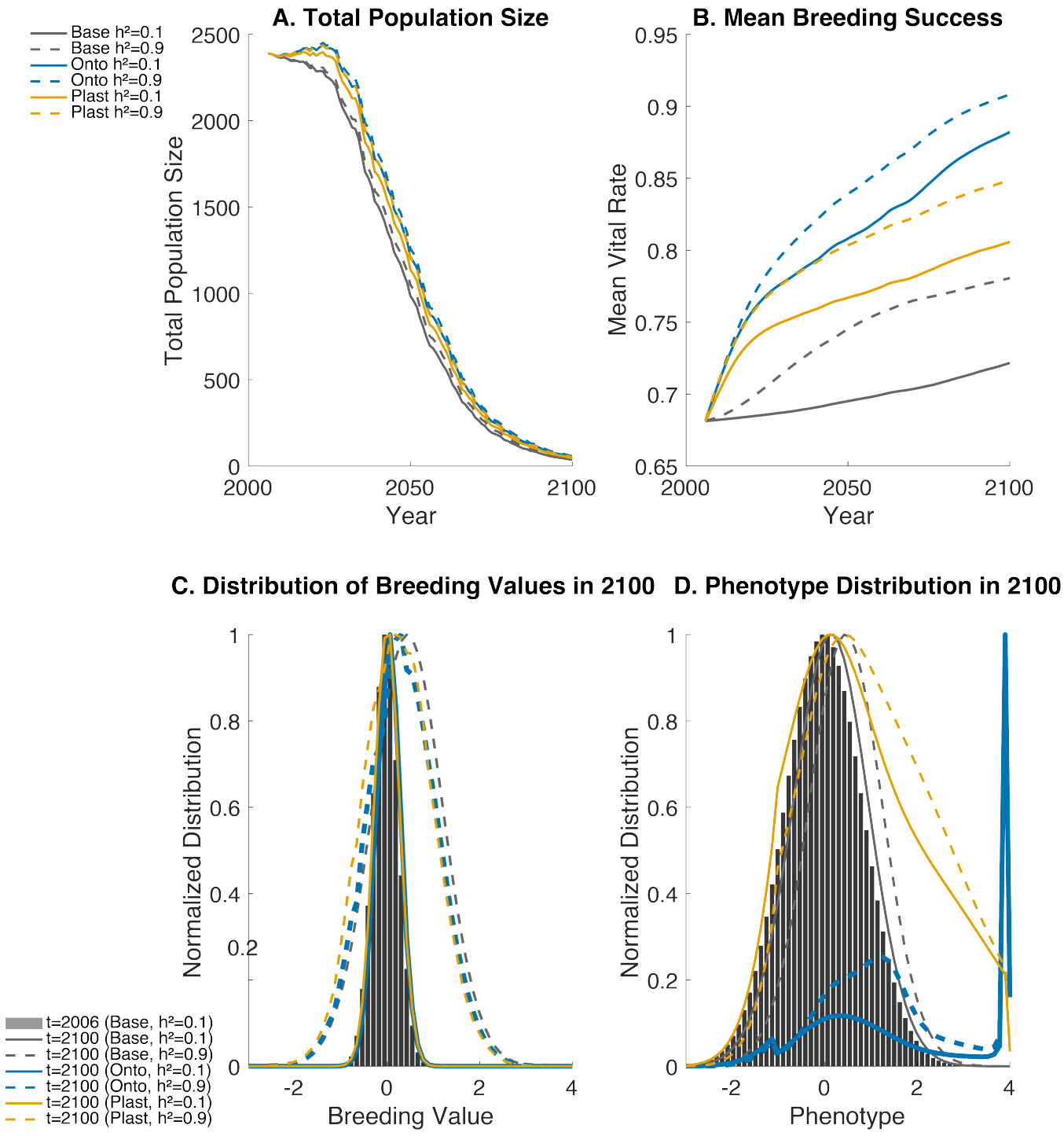

Fig. S5. Supplementary Figure S5. Eco-evolutionary dynamics of black-browed albatross traits under low-emissions climate projections, comparing scenarios of dynamic traits. We compare two heritability values: $h^2 = 0.1$ and 0.9. Solid lines represent $h^2 = 0.1$; dashed lines represent $h^2 = 0.9$. Foraging activity traits are dynamic and vary across years due to ontogeny (blue) or plastic responses to sea surface temperature (orange). (A,B) Demographic outcomes from 2006 to 2100. (C,D) Final (2100) and initial (2006) distributions of breeding value (C) and phenotype (D). Initial trait distributions are shown only for the baseline scenario with $h^2 = 0.1$ (gray bars).

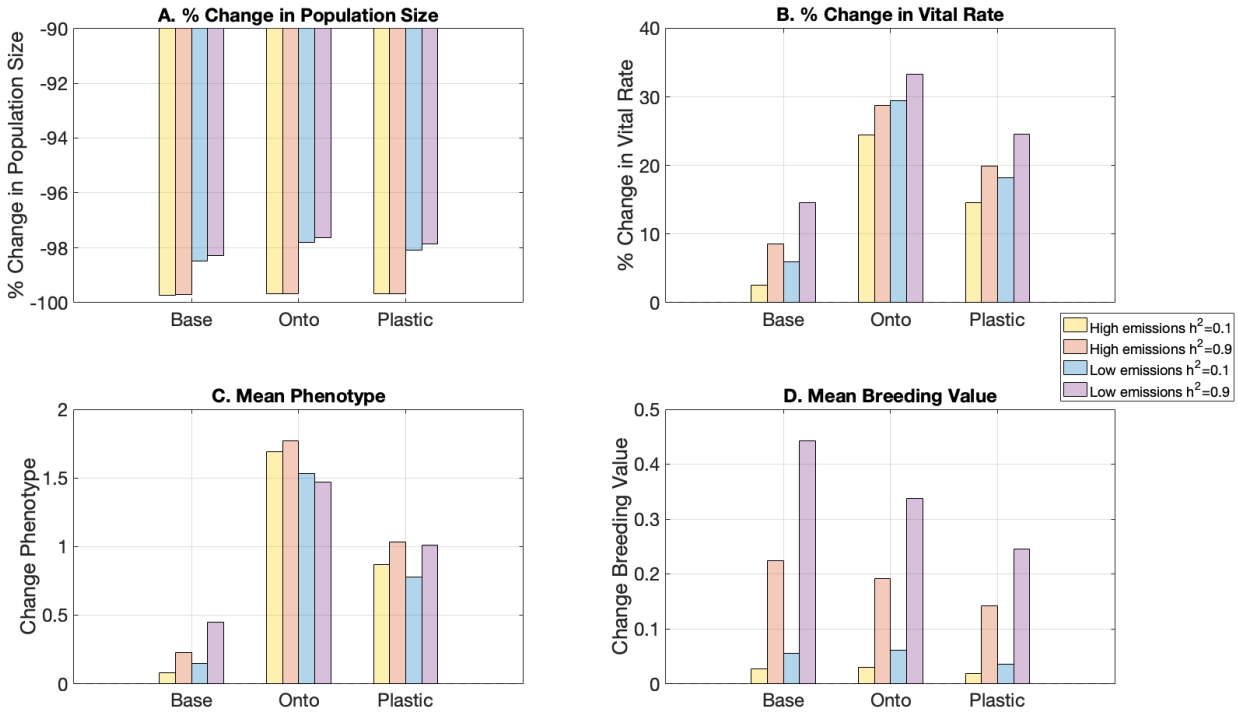

Fig. S6. Supplementary Figure S6. Trait-specific demographic and evolutionary responses across eco-evolutionary scenarios and climate emission pathways. Change values between year 2100 and 2006 for eco-evolutionary outcomes across three scenarios for dynamic foraging activity traits: baseline, ontogeny, and plasticity. Bars are colored by heritability (h^2) and emissions scenario: high emissions (yellow and orange), low emissions (blue and purple), high heritability (orange and purple), and low heritability (yellow and blue). (A) Percent change in total population size from 2006 to 2100. (B) Percent change in breeding success. (C) Change in phenotype from 2006 to 2100. (D) Change in breeding value from 2006 to 2100.

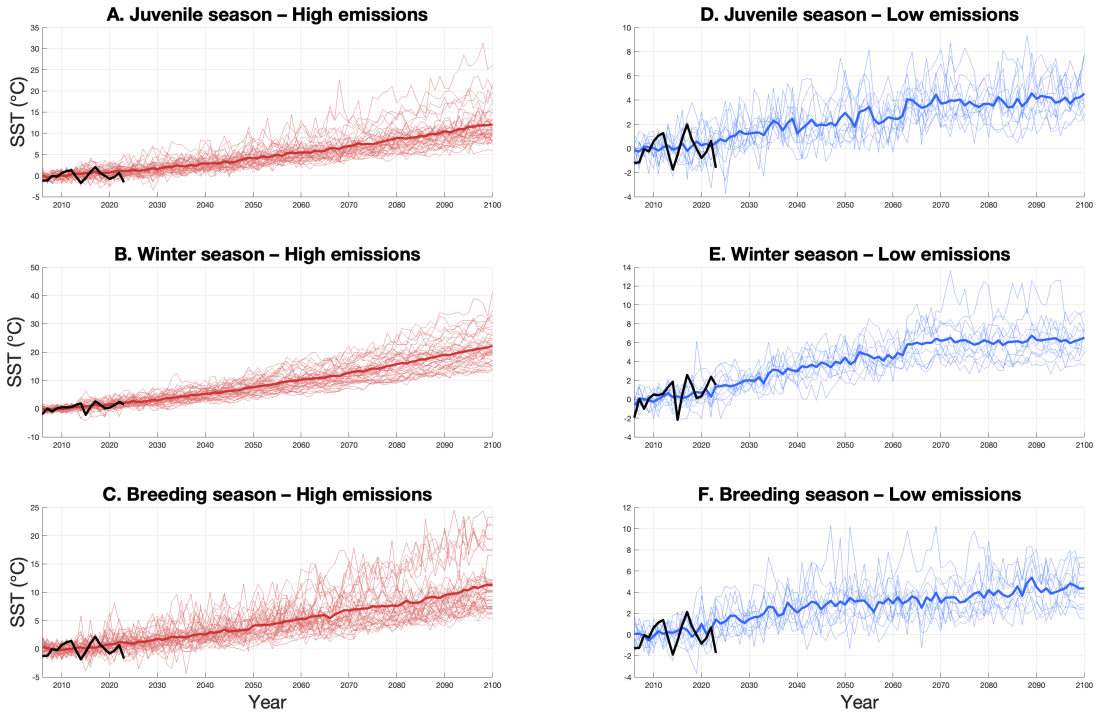

Fig. S7. Supplementary Figure S7. Seasonal sea surface temperature projections under contrasting emission scenarios. Projected sea surface temperatures (SST) during the juvenile, winter, and breeding seasons of the black-browed albatross life cycle under a high-emission scenario (CESM2-LE; left column) and a low-emission scenario consistent with the Paris Agreement (CESM1-CAM5 2.0°NE; right column). Thin colored lines represent individual ensemble members, thick lines show the ensemble mean, and the black line shows observed SST off the Kerguelen Plateau.

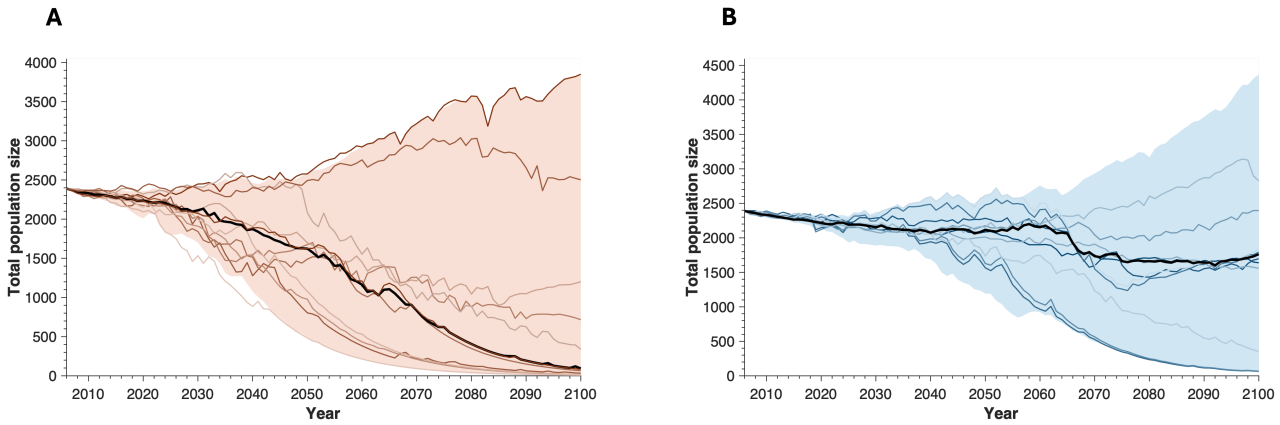

Fig. S8. Supplementary Figure S8. Eco-evolutionary dynamics of black-browed albatross populations under climate change. Projected total population size from 2006 to 2100 under (A) high-emissions climate projections and (B) low-emissions climate projections with sea surface temperature-dependent selection on juvenile survival. Projections account for uncertainty in demographic processes (measurement error and environmental stochasticity) and natural climate variability across ensemble members of Earth system model simulations, assuming heritability $h^2 = 0.3$. Thick black lines indicate the median projected population size, shaded areas denote 90% uncertainty envelopes, and thin colored lines represent individual stochastic population trajectories.

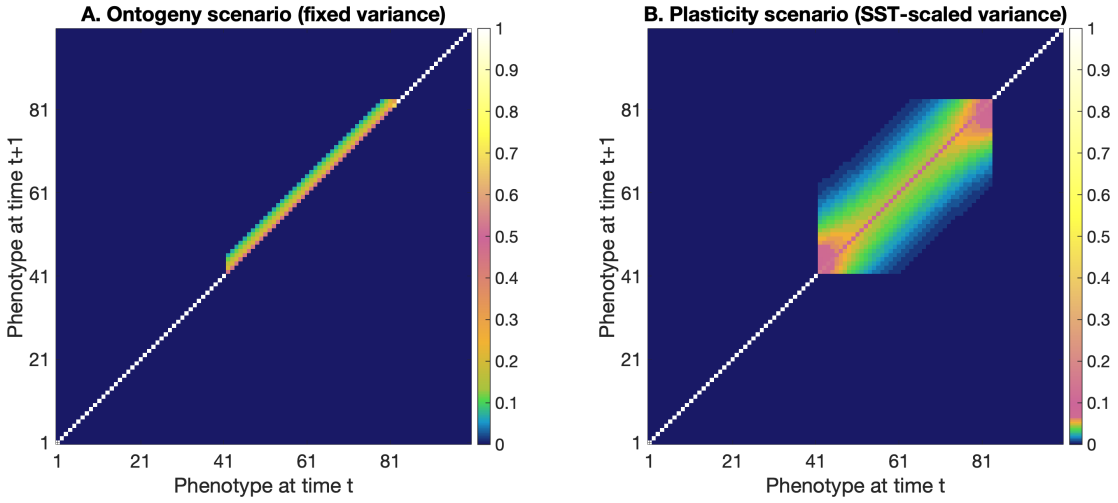

Fig. S9. Supplementary Figure S9. Phenotype transition matrices $\mathbf{P}_{i,j}$ for dynamic trait scenarios. Each matrix shows the probability of transitioning from a phenotype class at time t (x-axis) to a class at time $t+1$ (y-axis). (A) In the ontogeny scenario, phenotypes can gradually increase over time, simulating age- or experience-related improvement. (B) In the plasticity scenario, transitions are broader and environment-dependent, allowing more flexible shifts in phenotype in response to sea surface temperature variability. Transition probabilities are based on truncated Gaussian distributions and normalized by column. Color intensity reflects transition probability.

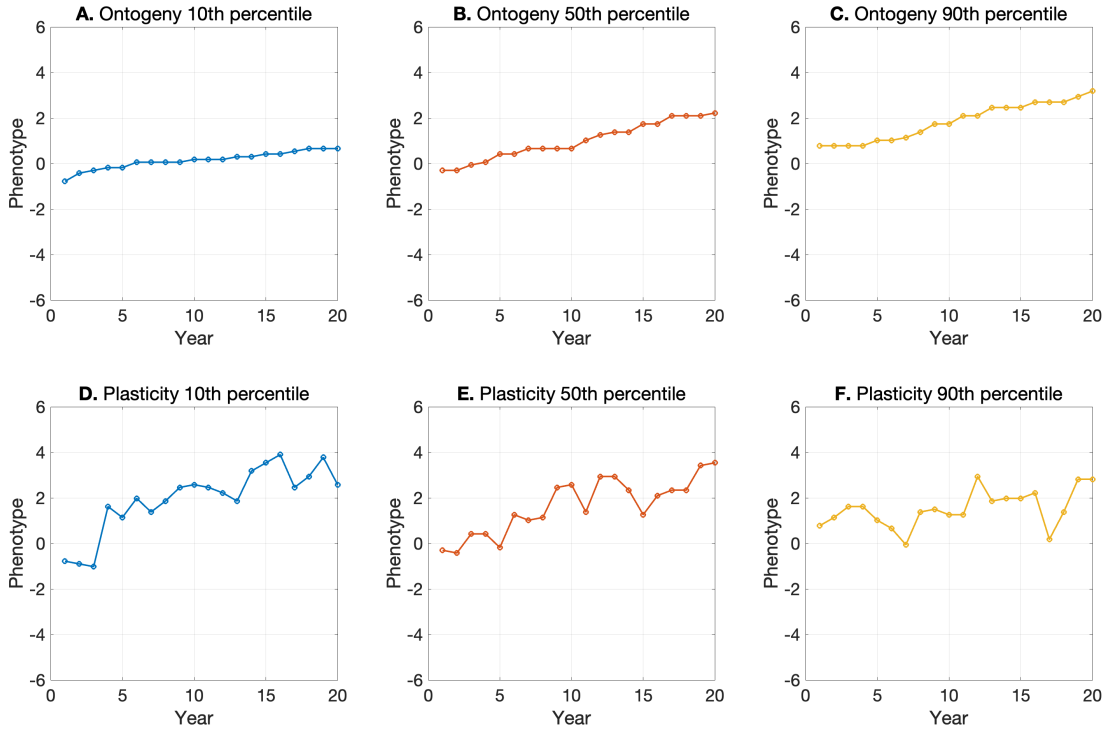

Fig. S10. Supplementary Figure S10. Individual trait trajectories under dynamic trait scenarios. This figure shows simulated phenotypic trajectories over 20 years for individuals starting in three different phenotype classes, corresponding to the 10th, 50th, and 90th percentiles of the observed distribution of foraging activity. (A–C) Ontogeny scenario: individuals begin in low, intermediate, or high trait classes and experience gradual, directional changes over time, reflecting age- or experience-related improvement. (D–F) Plasticity scenario: individuals show more variable trajectories, with transitions depending on environmental variability (e.g., sea surface temperature). Each line represents a single individual; points show yearly phenotype values sampled from the phenotype transition matrix $\mathbf{P}_{i,j}$ based on the previous year's state.

Exploring Phenotypic Plasticity and Ontogenetic Change

Several functional traits considered in this study are known to vary within individuals across years, particularly foraging and phenological traits such as activity, time spent on the water, and return date to the breeding colony. These traits were quantified using data from geolocator (GLS) deployments on breeding adults (2), providing detailed information on individual behavior and seasonal timing. The GLS dataset spans eight non-breeding seasons (2006–2013) and provides repeated behavioral and phenological measurements for individual birds (from 64 to 86 birds and 118 to 146 trips (2)), but typically over only one to a few years per individual. Although this represents a unique and rich dataset for characterizing individual-level behavioral variation, data availability remains limited in both temporal and environmental variability coverage. As a result, we were unable to detect robust and consistent statistical relationships linking trait variation to either climatic covariates or age across the full life cycle.

Given these limitations, the core analyses in the main text assume that phenotypic traits are fixed within individuals. Here, we relax this assumption to qualitatively explore the potential effects of phenotypic plasticity and ontogenetic change on eco-evolutionary population dynamics. Rather than attempting to estimate poorly constrained relationships, we adopt a scenario-based approach in which plastic and ontogenetic responses are specified. These scenarios are intentionally optimistic under future climate change, yet remain biologically reasonable, and are designed to explore upper bounds on the extent to which unmodeled plasticity or age-related improvement could alter conclusions regarding evolutionary rescue.

We analyzed two dynamic traits scenario (Fig. S9, S10):

1. **Ontogenic improvement**: foraging behavior improves with age and experience, as documented in many seabird species, especially during early life (20, 21), and

2. **Plastic response**: foraging behavior responds directly to environmental variation (22, 23).

Both require modifying the phenotype transition matrix $\mathbb{P}$ to allow individuals to shift between phenotypic classes over time. $\mathbf{P}_{ij}$ are transition matrices for individuals of stage i and in breeding value class j and of dimensions $p \times p$.

Truncated Gaussian distribution. In both scenarios, $G_{V_\mathrm{D}}(z_j - z_i)$ represents a truncated Gaussian kernel of the form:

$$G_{V_\mathrm{D}}(z_j - z_i) = \exp\left(-\frac{(z_j - z_i)^2}{2V_\mathrm{D}}\right) \cdot \mathbb{I}_{\{|z_j - z_i| < \delta_T\}} \cdot \mathbb{I}_{\{z_j, z_i \in [z_{\min}, z_{\max}]\}}, \quad [15]$$

where V_D is the variance, δ_T is the maximum allowed transition step, and $\mathbb{I}$ denotes indicator functions that ensure transitions are limited to a biologically plausible range and remain within the bounds of the observed phenotypic space. The directionality of transitions ($z_j \geq z_i$ vs. bidirectional) and the scaling of V_D differ between scenarios, but the general form of the kernel is the same. Columns of the resulting transition matrix are normalized such that $\sum_j P_{j,i} = 1$.

Ontogenetic Improvement. In the ontogeny scenario (Fig. S9**A**, S10**A,B,C**), we assume that individuals gradually improve their foraging behavior with age and experience. Transitions between phenotype classes are governed by a truncated Gaussian kernel:

$$G_{V_\mathrm{D}}(z_j - z_i), \quad [16]$$

where G_{V_D} is a Gaussian distribution centered at zero with variance V_D. Transitions are restricted to non-negative changes in phenotype (i.e., $z_j \geq z_i$) and to a maximum phenotypic increment $dT = 4\Delta z$, where Δz is the bin width of the phenotype distribution. Transitions outside the observed phenotypic range are not allowed. For each phenotype class i, the transition probabilities are normalized to sum to 1, and the resulting matrix $\mathbf{P}_{i,j}$ is repeated across all breeding value classes to construct the block-diagonal matrix $\mathbb{P}$.

Phenotypic Plasticity. In the plasticity scenario (Fig. S9**B**, S10**D,E,F**), phenotypic transitions are influenced by environmental conditions, allowing individuals to shift flexibly between phenotypic classes within their lifetime. We assume that greater environmental variability—e.g., fluctuations in sea surface temperature (SST)—induces broader phenotypic responses. To capture this, we scale the variance of the Gaussian transition kernel by the environmental gradient:

$$V_\mathrm{D} = \frac{z_{\max} - z_{\min}}{\Delta_{\mathrm{SST}}}, \quad [17]$$

where $z_{\min}$ and $z_{\max}$ are the bounds of the observed phenotypic distribution, and Δ_{SST} represents interannual SST variability. The transition probability is then modeled using a truncated Gaussian distribution:

$$G_{V_\mathrm{D}}(z_j - z_i), \quad [18]$$

but unlike the ontogeny scenario, we allow both upward and downward phenotypic shifts, with the kernel truncated over a symmetric or asymmetric interval around zero. This relaxation of directional constraints enables reversible changes in phenotype, consistent with plastic responses to variable environments.

Trait Dynamics Across Ontogeny and Environmental Plasticity. Figures S9 and S10 illustrate these dynamics. In the ontogeny scenario, transitions are constrained to gradual, unidirectional increases in phenotype, reflecting age- or experience-related improvement and appearing as a narrow band of light blue in the matrix (Fig. S9**A**). In contrast, the plasticity scenario permits more flexible shifts in either direction, with transition probabilities scaled by environmental variability (e.g., sea surface temperature), resulting in a wider band of transitions spanning from light blue to yellow (Fig. S9**B**).

To visualize individual-level outcomes, we simulated phenotypic trajectories over 20 years for individuals starting at the 10th, 50th, and 90th percentiles of the phenotypic distribution (Fig. S10). These examples highlight how ontogeny produces more predictable, directional changes, whereas plasticity yields greater interannual variability in trait expression.

Effects of Plasticity and Ontogenetic Change. The inclusion of dynamic foraging activity increased average breeding success, reaching values as high as 0.9 by 2100 compared to 0.72 in the baseline scenario (Fig. S5B). These high values by 2100 should be interpreted as an intentionally optimistic upper bound rather than realistic projections, designed to test whether even extreme improvements in adult performance could offset climate-driven demographic losses. Despite this strong increase in breeding success, the effect on overall population size remained negligible (Fig. S5A).

In terms of evolutionary dynamics, high heritability led to an increase in the mean breeding value (Fig. S6D) with a shift in its distribution: the mode moved from 0 in 2006 to 0.42 by 2100 (Fig. S5C). Breeding values are expressed on a standardized trait scale, where zero corresponds to the population mean at the start of the study period and positive values indicate genotypes associated with higher trait values and, consequently, higher expected demographic performance. In contrast, under low heritability, breeding values remained largely stable over time, with minimal changes in distribution.

Phenotypic distributions also shifted towards higher values over time when traits were assumed dynamic (Fig. S6C). Under the plasticity scenario, the proportion of individuals with higher foraging activity increased over time due to the assumed positive plastic response of activity level to SST (Fig. S5D). This resulted in a slightly broader bell-shaped distribution. In the ontogeny scenario, however, a bimodal distribution emerged by 2100, dominated by individuals expressing the highest level of activity. This pattern arose because when SST increases, overall juvenile survival and breeding probabilities decrease, leading to a strong demographic shift toward older age classes that have gradually gained foraging experience throughout their lifetime. Although these individuals may benefit from greater breeding success, because the overall breeding probabilities remain low, the production of new individuals was insufficient to sustain the population, ultimately leading to extinction.

Interestingly, the increase in mean breeding value from 2006 to 2100 was greater in the baseline trait scenario than in the ontogeny and plasticity scenarios (Fig. S6D). For illustration, under the low-emissions climate pathway and high heritability ($h^2 = 0.9$), the change in mean breeding value was 0.44 in the baseline scenario, compared with 0.34 under ontogeny and 0.25 under plasticity. This qualitative pattern—reduced evolutionary change when plastic or age-dependent responses are present—was consistent across climate scenarios and heritability values.

This pattern does not reflect stronger selection in the baseline case, but rather the fact that plastic and age-related improvements improve demographic performance, thereby reducing the strength of selection acting on heritable trait variation. In this sense, plasticity and ontogenetic change can mask selective pressures, slowing evolutionary change in breeding values even when overall trait values or vital rates improve (24–26).

References

1. S Jenouvrier, et al., Climate change and functional traits affect population dynamics of a long-lived seabird. *J. Anim. Ecol.* **87**, 906–920 (2018).
2. M Desprez, S Jenouvrier, C Barbraud, K Delord, H Weimerskirch, Linking oceanographic conditions, migratory schedules and foraging behaviour during the non-breeding season to reproductive performance in a long-lived seabird. *Funct. Ecol.* **32**, 2040–2053 (2018).
3. F Ventura, et al., The silent decline of the black-browed albatross across the southern ocean revealed through long-term demographic monitoring. Manuscript submitted (2025).
4. BM Sanderson, et al., Community climate simulations to assess avoided impacts in 1.5 and 2 c futures. *Earth Syst. Dyn.* **8**, 827–847 (2017).
5. JW Hurrell, et al., The community earth system model: A framework for collaborative research. *Bull. Am. Meteorol. Soc.* **94**, 1339–1360 (2013).
6. KB Rodgers, et al., Ubiquity of human-induced changes in climate variability. *Earth Syst. Dyn.* **12**, 1393–1411 (2021).
7. G Danabasoglu, et al., The Community Earth System Model Version 2 (CESM2). *J. Adv. Model. Earth Syst.* **12**, e2019MS001916 (2020).
8. V Eyring, et al., Overview of the Coupled Model Intercomparison Project Phase 6 (CMIP6) experimental design and organization. *Geosci. Model. Dev.* **9**, 1937–1958 (2016).
9. C Deser, A Phillips, V Bourdette, H Teng, Uncertainty in climate change projections: The role of internal variability. *Clim. Dyn.* **38**, 527–546 (2012).
10. JV de Walle, J Garnier, T Bonnet, S Jenouvrier, Toward a unified approach to modeling adaptation among demographers and evolutionary ecologists. *Methods Ecol. Evol.* (2025).
11. G Roth, H Caswell, Hyperstate matrix models: Extending demographic state spaces to higher dimensions. *Methods Ecol. Evol.* **7**, 1438–1450 (2016).

12. LE Kruuk, A Charmantier, D Garant, The study of quantitative genetics in wild populations. *Quant. genetics wild* pp. 1–15 (2014).
13. CM Hunter, H Caswell, The use of the vec-permutation matrix in spatial matrix population models. *Ecol. modelling* **188**, 15–21 (2005).
14. JP Bird, et al., Generation lengths of the world's birds and their implications for extinction risk. *Conserv. Biol.* **34**, 1252–1261 (2020).
15. L Lachs, et al., Natural selection could determine whether acropora corals persist under expected climate change. *Science* **386**, 1289–1294 (2024).
16. R Gomulkiewicz, RD Holt, When does evolution by natural selection prevent extinction? *Evolution* **49**, 201–207 (1995).
17. H Weimerskirch, M Louzao, S de Grissac, K Delord, Changes in wind pattern alter albatross distribution and life-history traits. *science* **335**, 211–214 (2012).
18. AJ Constable, et al., Climate change and southern ocean ecosystems i: how changes in physical habitats directly affect marine biota. *Glob. change biology* **20**, 3004–3025 (2014).
19. E Postma, Four decades of estimating heritabilities in wild vertebrate populations: improved methods, more data, better estimates? in *Quantitative genetics in the wild*, eds. A Charmentier, D Garant, LEB Kruuk. (Oxford University Press, Oxford), 1st edition, pp. 16–33 (2014).
20. F Daunt, S Wanless, MP Harris, L Money, P Monaghan, Older and wiser: improvements in breeding success are linked to better foraging performance in european shags. *Funct. Ecol.* **21**, 561–567 (2007).
21. L Riotte-Lambert, H Weimerskirch, Do naive juvenile seabirds forage differently from adults? *Proc. Royal Soc. B: Biol. Sci.* **280**, 20131434 (2013).
22. SC Patrick, et al., Individual differences in searching behaviour and spatial foraging consistency in a central place marine predator. *Oikos* **123**, 33–40 (2014).
23. SC Patrick, JG Martin, CC Ummenhofer, A Corbeau, H Weimerskirch, Albatrosses respond adaptively to climate variability by changing variance in a foraging trait. *Glob. Chang. Biol.* **27**, 4564–4574 (2021).
24. LM Chevin, R Lande, GM Mace, Adaptation, plasticity, and extinction in a changing environment: towards a predictive theory. *PLoS biology* **8**, e1000357 (2010).
25. L Chevin, J Bridle, Impacts of limits to adaptation on population and community persistence in a changing environment. *Philos. Transactions Royal Soc. B* **380**, 20230322 (2025).
26. RJ Fox, JM Donelson, C Schunter, T Ravasi, JD Gaitán-Espitia, Beyond buying time: the role of plasticity in phenotypic adaptation to rapid environmental change. *Philos. Transactions Royal Soc. B: Biol. Sci.* **374**, 20180174 (2019).